

pubs.acs.org/JPCA Article

# Comparative Thermodynamic and Structural Analysis of Polyfluorinated Dodecylphosphonic Acid Adsorption to Distilled and River Water Interfaces

Published as part of The Journal of Physical Chemistry virtual special issue "Early-Career and Emerging Researchers in Physical Chemistry Volume 2".

Andrew P. Carpenter,\* Jade N. White, Annemarie Hasbrook, Makenna Reierson, and Joe E. Baio



Cite This: https://doi.org/10.1021/acs.jpca.3c01487



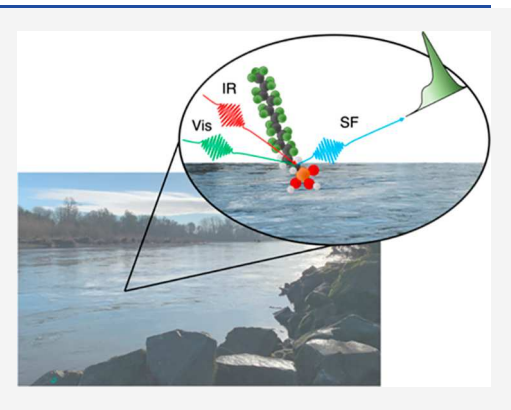
**ACCESS** 

Metrics & More

Article Recommendations

s Supporting Information

**ABSTRACT:** As concerns rise about the health risks posed by perand polyfluoroalkyl substances (PFAS) in the environment, there is a need to understand how these pollutants accumulate at environmental interfaces. Untangling the details of molecular adsorption, particularly when there are potential interactions with other molecules in environmental systems, can obscure the ability to focus on a particular contaminant with molecular specificity. Often adsorption studies of environmental interfaces require a reductionist approach, where laboratory experiments may not be fully tractable to environmental systems. In this work, we study polyfluorinated dodecylphosphonic acid ( $F_{21}$ -DDPA) at the aqueous surfaces of distilled water (the most reduced "environmental" surface) and river water to explore the use of vibrational sum-frequency (VSF) spectroscopy as an experimental probe of fluorinated contaminants at natural environmental surfaces. We demonstrate how VSF spectroscopy offers advantages over nonspecific



surface tension measurements when measuring PFAS adsorption isotherms at river water surfaces. VSF spectra of the C-F stretching region selectively probe the presence of F<sub>21</sub>-DDPA and can be used to extract meaningful structural insights and calculate surface concentrations, even at the complex river water surface. This study highlights the potential for VSF spectroscopy to be developed as a probe of fluorinated contaminants at natural environmental interfaces.

# **■ INTRODUCTION**

Concerns over PFAS accumulation in the environment have resulted in a sudden increase in efforts to understand their environmental prevalence, their impact on human health, and their breakdown and remediation. 1-5 Leaching of PFAS into groundwater sources results in their eventual transport to surface waters where the risk of human contact increases due to their accumulation in biomass and at aqueous surfaces. 6 The EPA has set strict guidelines for PFAS background levels, where some species should not exceed 0.02 ppt. Yet, water concentrations near contamination sources can be in significant excess of this limit and reach 100s to 1000s of  $\mu$ g/L.<sup>8,9</sup> Being highly surface active, PFAS have the capacity to accumulate within saturated and unsaturated zones in subsurface environments, foams, and the interfaces of surface waters.<sup>3,10–12</sup> These surfaces become potential PFAS sinks, making it important to understand their surface activity to accurately model their fate and transport throughout the environment.

Yet, studying PFAS adsorption behavior directly at environmentally relevant surfaces is not entirely straightforward. Under the Framework for Relevance And Methods Evaluation (FRAME) scheme used to define "environmental relevance", the experimental conditions of the background matrix are considered to span from ultrapure H<sub>2</sub>O to the complex aquatic matrix of naturally occurring water sources. <sup>13</sup> Often, PFAS adsorption phenomena are studied in a laboratory setting using surface tensiometry. <sup>10,14</sup> Due to the technique's nonspecific nature, a reductionist approach is required to untangle the impact the background aquatic matrix (e.g., ions, dissolved organic matter) exerts on pollutant adsorption and accumulation at aquatic surfaces. <sup>12,15,16</sup> Such studies will control the solution conditions by tuning the ionic strength and dissolved organic matter (DOM) using commercially available chemicals. While these studies can provide important mechanistic insights into PFAS surface activity, the FRAME scheme

Received: March 3, 2023 Revised: June 29, 2023



highlights that these findings may not always be directly transferable or relevant under actual environmental conditions. At the same time, however, the same framework also acknowledges the challenges and complexity of applying certain analytical tools and the limited nature of mechanistic insights that are possible from studying the complex environmental matrix. As such, a potential experimental technique that could provide experimental tractability on complex environmental surfaces is desirable.

It would be advantageous to identify experimental methods capable of isolating PFAS signatures at complex aqueous surfaces to interrogate PFAS directly at environmental interfaces. Toward this end, we investigate whether vibrational sum-frequency (VSF) spectroscopy could be used to directly interrogate PFAS at natural environmental surfaces amidst a complex aquatic matrix. VSF is a surface-specific spectroscopic technique that measures surface molecules' vibrational spectrum without contribution from bulk molecules. <sup>17</sup> The unique nature of the C-F stretching modes provide the possibility of resolving PFAS spectral features amidst an environmental matrix that would otherwise have interfering signatures from background DOM (e.g., humic acid) in the alkyl, carboxyl, or carbonyl vibrational regions. 18,19 Interestingly, studies of the C-F spectral region are conspicuously rare despite nearly 35 years of research using VSF spectroscopy. Thus, there is an opportunity to assess the possibility of applying VSF spectroscopy to probe PFAS behavior at the surface of a complex aquatic matrix.

Herein we study the adsorption of polyfluorinated dodecylphosphonic acid (F21-DDPA) at the two end points of potential solution conditions identified under the FRAME scheme: the ultrapure water surface and the surface of a complex environmental matrix. For the natural environmental surface, water is collected from a local river and remains unprocessed beyond filtration of larger sediment. The adsorption behavior of F21-DDPA is first studied at both interfaces by using surface tensiometry for different protonation states of the phosphonic headgroup. From these experiments the ability to calculate physical quantities, such as surfactant surface densities, is assessed for each surface. Next, VSF spectroscopy is used to measure the vibrational spectra of F<sub>21</sub>-DDPA at both aqueous surfaces. Results show that while the nonspecific surface tension measurements are complicated by the river water's solution matrix, VSF provides significant opportunities to study PFAS adsorption behavior with a molecular specificity in these complex environments.

## MATERIALS AND METHODS

**Chemicals and Solution Preparation.** The PFAS studied in this work, (3,3,4,4,5,5,6,6,7,8,8,9,9,10,10,11,11,12,12,12-heneicosafluorododecyl)phosphonic acid (MilliporeSigma), referred to herein as  $F_{21}$ -DDPA, was used as received without further purification. Aqueous subphases were either ultrapure water (18. MΩ·cm, Millipore Direct-Q3 System), termed DI-H<sub>2</sub>O, or river water collected from the Willamette River (Oregon, USA), termed WR-H<sub>2</sub>O. Water taken from the Willamette River was collected at the Willamette Boat Landing (Corvallis, OR) in 200 mL glass bottles and filtered (Corning 150 mL Polystyrene Filter System, 0.22 μm) prior to use as a subphase in surface tensiometry and spectroscopic studies. The most recent water quality report for the Willamette River is provided in the Supporting Information. All pH adjustments were done using a concentrated NaOH solution made from

NaOH tablets (ACS grade, Macron) dissolved in DI-H<sub>2</sub>O. Stock solutions of F<sub>21</sub>-DDPA were prepared at concentrations of  $\sim$ 30  $\mu$ M in neutral pH conditions for DI-H<sub>2</sub>O and 1 mM under basic pH conditions (pH  $\sim$  13) for both aqueous subphases. The pH values of all solutions were verified with pH indicator strips (VWR, Germany).

**Surface Tensiometry.** Surface tension measurements at the DI-H<sub>2</sub>O and WR-H<sub>2</sub>O surfaces were recorded using the Wilhelmy plate surface tensiometry methodology. For this, a DyneProbe (Kibron) was suspended from a Delta Pi tensiometer arm (Kibron) over homemade circular Teflon troughs. The surface tension of the bare air-water interface was recorded for both the DI-H2O and the WR-H2O subphases before the addition of any F21-DDPA. These bare surface tension values were used to calculate the surface pressure for each concentration of F<sub>21</sub>-DDPA, which is equal to the surface tension of the bare interface minus the surface tension of the interface with adsorbed F<sub>21</sub>-DDPA. After the addition of F21-DDPA to the aqueous subphase the typical time for the surface tension to equilibrate was ~10 min, with surface equilibration defined as the point when any changes in surface tension were <0.1 mN/m for at least a minute. Across all measurements, the average room temperature was measured to be 22.8  $\pm$  0.2 °C.

Vibrational Sum-Frequency Spectroscopy. The spectrometer used for all vibrational sum-frequency (VSF) spectroscopy experiments will be briefly described, as it is a commercially available system from EKSPLA (Lithuania). A 1064 nm fundamental beam is generated from an ND:YAG laser at a repetition rate of 50 Hz and a pulse width of 30 ps. This beam is frequency doubled to 532 nm where a portion of the 532 nm beam is split off and sent to the interface, while the rest is directed into an optical parametric amplifier and combined with the remaining 1064 nm beam to generate a frequency tunable IR pulse (1000–4000 cm<sup>-1</sup>). The generated IR beam is then sent to the air—water interface.

The 532 nm beam that is sent to the interface is hereafter termed the VIS beam. Before reaching the air—water interface, the polarization of the VIS beam is selected using a half-wave plate. The polarization of the IR beam is set by using a motorized periscope. The VIS and IR beams overlapped at the surface of aqueous solution contained within a homemade circular Teflon trough with incident angles of 60° and 54°, respectively. Sum-frequency photons that are generated at the surface are polarization selected by a half-wave plate and a Glan—Taylor polarizer cube before being spectrally dispersed with a monochromator onto a photomultiplier tube.

Every spectrum reported in this work has been averaged from normalized spectra recorded across multiple days that were collected with a step size of 2 cm<sup>-1</sup> and 100 shots per step. Spectra were normalized by the product of the VIS and IR beam intensities, which were recorded at every IR frequency. The analysis of VSF spectra is performed through a combination of spectra fitting. Normalized sum-frequency spectra were fit using the following equations:

$$I_{\rm SF} = |\chi_{\rm Total}^{(2)}|^2 I_{\rm VIS} I_{\rm IR} \tag{1}$$

$$\chi_{\text{Total}}^{(2)} = \chi_{\text{NR}}^{(2)} + \chi_{\text{Resonant}}^{(2)}$$
(2)

These equations describe how the VSF signal measured from the air—water interface  $(I_{\rm SF})$  is dependent on the intensities of the VIS and IR beams and the total second-order susceptibility

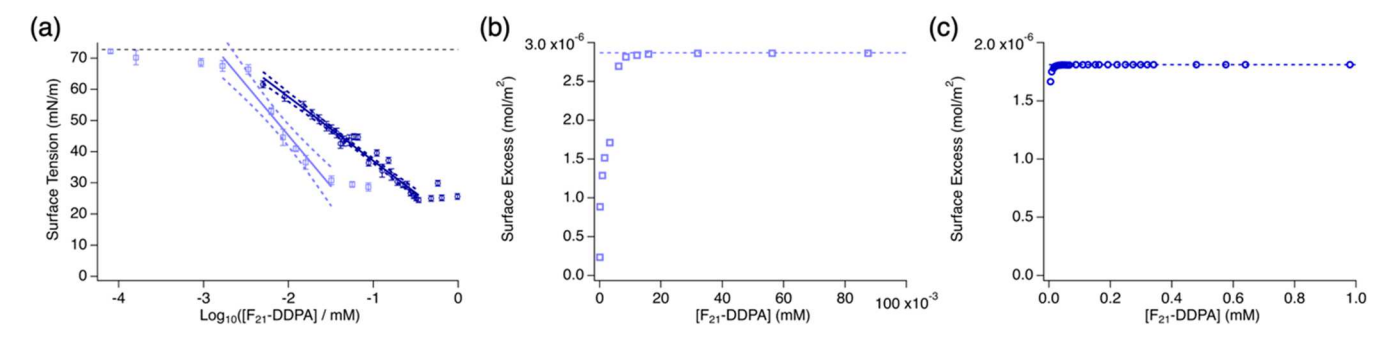


Figure 1. (a) Surface tension isotherms of  $F_{21}$ -DDPA adsorbed to the neutral (light blue squares) and basic (dark blue circles) surfaces. Gibbs adsorption fit (solid lines) and the 95% confidence bounds (dashed lines) are overlaid on top of the experimental data, while the horizontal dashed line marks the surface tension of the bare DI- $H_2O$  surface (72.8 mN/m). For the (b) neutral and (c) basic DI- $H_2O$  surfaces, surface excess values were calculated from the Frumkin equation (data points) using the maximum surface excess calculated from the Gibbs adsorption fit (dashed horizontal lines).

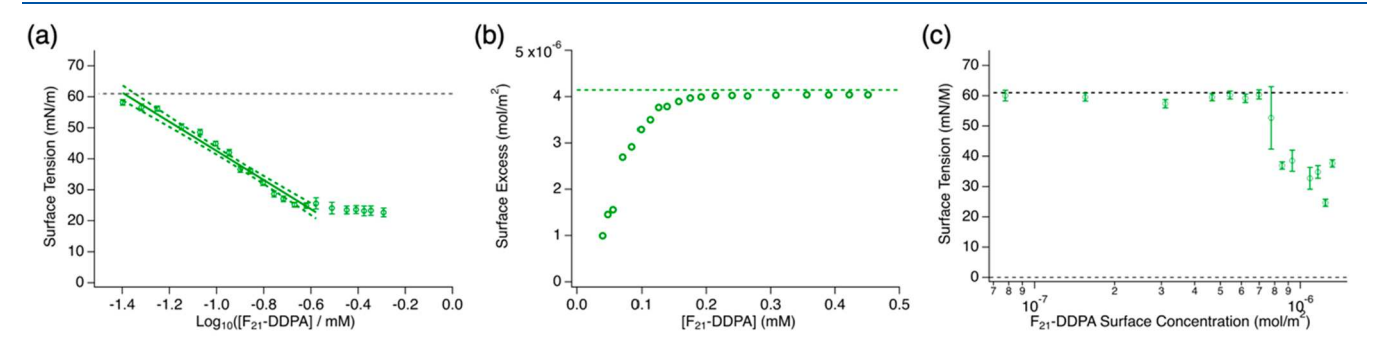


Figure 2. (a) Surface tension isotherm of  $F_{21}$ -DDPA adsorbed on the basic DI- $H_2O$  surface. Gibbs adsorption fit (solid line) and the 95% confidence bounds (dashed lines) overlay the experimental data, while the horizontal dashed line marks the average surface tension of the bare WR- $H_2O$  surface (61.0 mN/m). (b) Surface excess values for  $F_{21}$ -DDPA adsorbed on the basic WR- $H_2O$  surface were calculated from the Frumkin equation (data points) using the maximum surface excess calculated from the Gibbs adsorption fit (dashed horizontal lines). (c) Surface tension values for F21-DDPA at the neutral WR- $H_2O$  surface tension of the bare surface is marked by a horizontal dashed line.

of the surface  $(\chi_{\rm NR}^{(2)})$ . The total second-order susceptibility contains both nonresonant  $(\chi_{\rm NR}^{(2)})$  and resonant  $(\chi_{\rm Resonant}^{(2)})$  contributions. While higher-order contributions sometimes manifest in VSF spectra, <sup>20</sup> such as from bulk solvent molecules, these have been left out of our analysis because H<sub>2</sub>O molecules do not have any vibrational modes in the spectral region measured here. Thus, the final form of our fitting routine that accounts for both nonresonant and resonant contributions takes the following form:

$$\chi_{\text{Total}}^{(2)} = A_{\text{NR}} e^{i\varphi} + \sum_{n} \frac{A_{n}}{\omega - \omega_{n} + i\Gamma_{n}}$$
(3)

Within eq 3 the nonresonant contributions are modeled with a frequency-independent amplitude  $(A_{NR})$  and an associated phase factor  $(\varphi)$ , while the n vibrational resonances are modeled using a series of Lorentzian line shapes that each contain a vibrational amplitude  $(A_n)$ , frequency  $(\omega_n)$ , and line width  $(\Gamma_n)$ . Igor Pro (ver. 8.04, Wavemetrics) was used for all VSF fitting analysis.

**Quantum Chemical Calculations.** Previous studies have reported mixed results in using density functional theory (DFT) methods to aid in the analysis of C–F stretching SFG spectra. Within this work, the open source quantum chemistry program, ORCA (ver. 5.0.0),  $^{23,24}$  was used to carry out DFT calculations using the B3LYP functional  $^{25,26}$  with the 6-31G(d) basis set. Prior to these calculations, the molecular structure of  $F_{21}$ -DDPA was geometry optimized where a helical structure was observed in the alkyl chain, consistent with

experimental results of the structure of perfluorinated hydrocarbons.  $^{27}$ 

## ■ RESULTS AND DISCUSSION

Adsorption of  $F_{21}$ -DDPA to Environmental Aqueous Surfaces. As mentioned above, DI-H<sub>2</sub>O and WR-H<sub>2</sub>O represent the two end points of potential solution conditions under the FRAME scheme. We first assess the information that can be calculated from surface tension measurements of  $F_{21}$ -DDPA at both aqueous surfaces before investigating the potential of VSF spectroscopy to study PFAS adsorption at complex aqueous surfaces and its potential to measure adsorption isotherms. Possessing a phosphonic headgroup, the first and second  $pK_a$  of  $F_{21}$ -DDPA are estimated to be below 3 and 8.3, respectively, from the available data on hydrogenated n-dodecylphosphonic acid (DDPA). To investigate the adsorption behavior of both deprotonated states of  $F_{21}$ -DDPA, surface tension measurements were performed at the neutral and basic (pH = 13) surfaces.

At the DI- $H_2O$  surface,  $F_{21}$ -DDPA adsorption was studied by using the Wilhelmy plate surface tensiometry methodology. At both pH values, the surface tension is observed to decrease as the bulk  $F_{21}$ -DDPA concentration is increased (Figure 1). Being the most simplified aqueous surface, the analysis of this data is relatively straightforward.  $F_{21}$ -DDPA is observed to be more surface active when the headgroup is singly protonated under neutral pH conditions (light blue squares, Figure 1a) compared to its fully deprotonated form in basic solution (dark

blue squares, Figure 1a). The thermodynamically derived Gibbs adsorption equation was used to calculate the maximum surface excess for both isotherms (Figure 1a). At neutral pH, the maximum surface excess was calculated to be 2.9 ( $\pm 0.8$ ) ×  $10^{-6}$  mol/m², whereas the maximum surface excess was calculated to be 1.8 ( $\pm 0.2$ ) ×  $10^{-6}$  mol/m² at a basic pH. These values correspond to an average area per molecule of 58 and 92 Ų/molecule, respectively, indicating the F<sub>21</sub>-DDPA monolayer packs more tightly when the headgroup possesses a charge of -1 in neutral conditions compared to a charge of -2 under basic conditions.

At both surfaces, F21-DDPA appears to exhibit "ideal", Langmuir-type, adsorption behavior. This is similar to the adsorption isotherms typically observed for common ionic and nonionic hydrogenated surfactants and some PFAS at aqueous surfaces. 12,29,30 Due to the appearance of Langmuir-type adsorption behavior, the Frumkin equation was used to estimate the F21-DDPA surface excess from the calculated surface pressures (Figure 2b,c).<sup>29</sup> At the neutral pH surface the estimated surface excess was calculated to vary from (0.2-2.9)  $\times$  10<sup>-6</sup> mol/m<sup>2</sup>, which is 8–100% the maximum surface excess. Meanwhile, at the basic DI-H2O surface, the surface excess is estimated to vary from  $(1.6-1.8) \times 10^{-6}$  mol/m<sup>2</sup>, 90-100% the maximum surface excess. At the neutral surface, F<sub>21</sub>-DDPA quickly saturates the surface, while a much larger increase in bulk concentration only shifts the surface concentration from 90 to 100% under basic pH conditions.

The protonation state clearly influences the surface activity, with  $F_{21}$ -DDPA being less surface active when it possesses a larger headgroup charge. This pH dependence will also impact the CMC. For the singly protonated state, the CMC is calculated to be 27  $\mu$ M, while it is calculated to be 364  $\mu$ M for the fully deprotonated state (see the Supporting Information for details). Both of these are a reduction from the CMC's reported for DDPA, ~100 and ~600  $\mu$ M, respectively. The observed reduction in CMC, in addition to surface tension saturating at concentrations ~10× lower than common ionic hydrogenated surfactants (e.g., SDS, CTAB, AOT, etc.), 32–34 is to be expected as a result of the fluorinated chains' increased hydrophobicity. 35,36

While the kinds of information (i.e., surface concentration and CMC) calculated in the above analysis are readily attainable for the DI-H2O surface, similar analyses will be frustrated at the surface of water taken directly from the Willamette River. For these experiments, the WR-H<sub>2</sub>O was initially filtered to remove larger sediment, and no further purification procedures were performed. Thus, the filtered solution is still likely to contain significant concentrations of ions and DOM. As such, this solution is representative of the complex matrix end of the experimental conditions pillar within the FRAME scheme. The pH of the WR-H<sub>2</sub>O was tested post filtration and confirmed to be between pH 7-7.5, consistent with recent historic pH trends of the Willamette River near Corvallis, OR (see the Supporting Information). It is also consistent with the pH measured for the DI-H<sub>2</sub>O. While F<sub>21</sub>-DDPA was soluble in a basic WR-H<sub>2</sub>O solution, solubilizing F<sub>21</sub>-DDPA in neutral WR-H<sub>2</sub>O failed despite the headgroup being partially deprotonated and charged at this pH. The reduction of solubility is likely the result of the inorganic matter remaining in the WR-H<sub>2</sub>O, postfiltration. One would expect F<sub>21</sub>-DDPA to have similar properties to a hydrogenated surfactant with a longer alkyl chain (>20 carbons long)35,36 which will have a high Krafft temperature. For the

singly protonated form of  $F_{21}$ -DDPA, the Krafft temperature has likely been raised above our experimental temperature by the presence of salt,<sup>37</sup> making micelle formation not possible and causing  $F_{21}$ -DDPA to precipitate out of solution.

At the bare WR-H<sub>2</sub>O surface, the surface tension was measured to be  $61.0 \pm 4.0$  mN/m for both pH conditions. This value is more than 10 mN/m below that of the neat DI-H<sub>2</sub>O surface (72.8 mN/m), indicating that residual organic matter in the WR-H2O subphase, likely DOM, is adsorbing to the aqueous surface. For a basic WR-H<sub>2</sub>O solution in which F<sub>21</sub>-DDPA can be readily solubilized, a sharp decrease in the surface tension was observed as the bulk concentration was increased (Figure 2a). An application of the Gibbs adsorption equation (solid line, Figure 2a) produces a reasonable maximum surface excess of 4.1 ( $\pm 0.4$ )  $\times$  10<sup>-6</sup> mol/m<sup>2</sup>. This corresponds to a maximum surface density of 40 Å<sup>2</sup>/molecule, which is approximately twice the surface density relative to the basic DI-H<sub>2</sub>O surface. Again, the surface tension isotherm appears to exhibit Langmuir-type behavior, and therefore the surface excess was estimated using the Frumkin equation (Figure 2b). The calculated surface excess values range from  $(1.0-4.1) \times 10^{-6} \text{ mol/m}^2 (25-100\% \text{ the maximum surface})$ excess). These calculated surface concentrations appear reasonable, despite the analysis ignoring the presence of DOM in WR-H<sub>2</sub>O solutions. While one might reasonably expect the surface concentration to change in the presence of ions and DOM, it would be inappropriate to assign surface tension changes, from which the surface concentrations are calculated, solely to F<sub>21</sub>-DDPA. To account for the effects of DOM adsorption, the surface activity of background DOM needs to be determined, and the simplest accounting of these effects would consider them additive to  $F_{21}$ -DDPA adsorption. However, it is likely that DOM surface activity changes are not constant but rather will vary with F<sub>21</sub>-DDPA concentration. Such synergistic effects are commonly seen in surfactantpolymer and mixed surfactant systems. 38-40 Without understanding the adsorption behavior of the DOM, it is impossible to untangle the specific F<sub>21</sub>-DDPA surface concentrations from the surface tension data.

To study F<sub>21</sub>-DDPA adsorption to the neutral WR-H<sub>2</sub>O surface, F21-DDPA was dissolved in a 1:3 methanol:CHCl3 mixture (final concentration of 0.375 mg/mL) to overcome the solubility issues observed for the neutral WR-H<sub>2</sub>O solution. The organic solvated F21-DDPA solution was then added dropwise to the surface of a neutral WR-H2O solution, similar to how lipid monolayers are constructed at the air—water interface. The results of these measurements are shown in Figure 2c, where the surface pressure is plotted against the added surface concentration (assuming no F21-DDPA dissolves into the subphase). The surface pressure seems to be quite insensitive to the presence of F<sub>21</sub>-DDPA until a concentration of  $\sim 7 \times 10^{-7}$  mol/m<sup>2</sup> is reached, where a sudden decrease and then a plateau in the surface tension is observed. This adsorption behavior is quite unlike the adsorption behavior of typical surfactants, highlighting that surface tensiometry studies of F<sub>21</sub>-DDPA at the natural environmental surface are complicated by the nonspecific nature of the measurement when background DOM and ions are present. With such adsorption behaviors as we have observed at the WR-H2O surface, a molecularly specific probe would greatly benefit the study of pollutant adsorption from complex aquatic matrices by providing F<sub>21</sub>-DDPA specific information amidst background DOM.

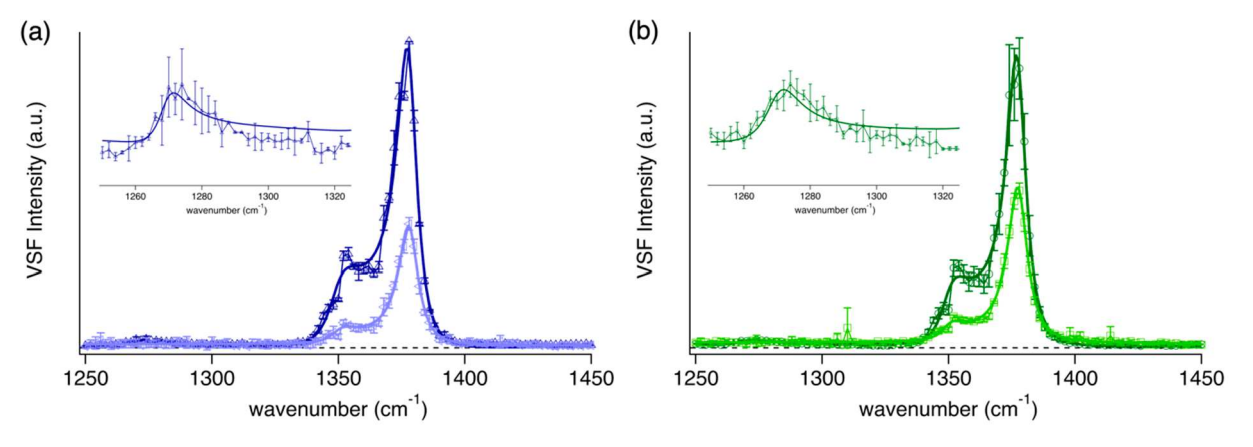


Figure 3. VSF spectra of  $F_{21}$ -DDPA at the basic air—water interfaces. (a) At the DI- $H_2O$  surface, normalized SSP (light blue, left triangles) and PPP (dark blue, triangles) spectra are shown with an expanded view (25×) of the low intensity resonance near 1270 cm<sup>-1</sup> in the PPP spectrum. (b) At the WR- $H_2O$  surface, normalized SSP (light green, squares) and PPP (dark green, circles) spectra are shown with an expanded view (25×) of the low intensity resonance near 1270 cm<sup>-1</sup> in the PPP spectrum.

Vibrational Sum-Frequency Studies of F21-DDPA at Aqueous Surfaces. While surface tensiometry measurements are unable to distinguish contributions from individual components within a complex aqueous solution, the molecular and surface specificity provided by VSF spectroscopy has the potential to isolate the unique spectral signatures of surfaceadsorbed PFAS amidst other interfacial species. Despite the present popularity of VSF spectroscopy, published VSF spectra of the C-F stretching region (defined here as 1250-1450 cm<sup>-1</sup>)<sup>43</sup> are uncommon, and the majority have focused on fluorinated polymer surfaces and not fluorinated surfactants at aqueous surfaces. 21,22,44-46 The vibrational features of the C-F stretching region are expected to be unique to F<sub>21</sub>-DDPA, and PFAS more broadly, provided the Willamette River is in accordance with the EPA's guidelines for background PFAS levels in water sources. Thus, to explore whether VSF can isolate F<sub>21</sub>-DDPA's spectral features at the surface of a complex aquatic matrix, we recorded C-F stretching spectra at the WR-H<sub>2</sub>O surface in multiple polarization combinations and compared it with spectra recorded at the DI-H2O surface (Figure 3). Spectra were recorded for basic 0.5 mM F<sub>21</sub>-DDPA solutions, as F<sub>21</sub>-DDPA adsorbs from the bulk to both the DI-H<sub>2</sub>O and WR-H<sub>2</sub>O surfaces under basic pH conditions. VSF spectra were recorded in the SSP and PPP polarization combinations, as multiple polarization combinations allow for conclusions to be drawn as to the orientation of interfacial species. At both surfaces, a strong VSF signal is observed between 1350 and 1400 cm<sup>-1</sup> in both polarization combinations. An additional, weaker vibrational mode is also observed in the PPP polarization combination near 1270 cm<sup>-1</sup> (insets, Figure 3). No resonant intensity was measured in SPS and, therefore no spectrum is reported for that polarization combination.

To interpret these VSF spectra, all spectra were fit with a series of Lorentzian lineshapes. Previous heterodyned VSF measurements of fluoroalkyl acrylate polymer surfaces and perfluorononionic acid (PFNA) identified three distinct vibrational resonances near 1350, 1370, and 1400 cm<sup>-1</sup> that could be attributed to different delocalized vibrational modes throughout the fluorinated alkyl chains. <sup>21,22</sup> In our spectra we do not observe any intensity near 1400 cm<sup>-1</sup> because this mode arises from the PFNA carboxylate headgroup, which is absent in our phosphonic acid surfactant. Therefore, the strong

VSF intensity between 1350 and 1400 cm<sup>-1</sup> is fit with two resonant modes, and the weak band in the PPP spectrum is fit with a single resonant mode. The SSP and PPP spectra were globally fit for each surface, with fit results placing the vibrational frequencies at 1270, 1350, and 1378 cm<sup>-1</sup>. Because of the strong intramolecular couplings in this frequency region, characterizing vibrational bands as strictly being a CF<sub>2</sub> or CF<sub>3</sub> mode is not reasonable. Thus, the three vibrational bands are hereafter termed modes 1, 2, and 3, respectively. In each spectrum the best fit has mode 2 and mode 3 possessing opposite phases, consistent with heterodyne VSF measurements.<sup>22</sup> While only observed in the PPP spectrum, spectral fits indicate mode 1 is in phase with mode 2 and out of phase with mode 3. A full list of these fit parameters is provided in the Supporting Information.

In VSF spectroscopy, the orientations of specific functional groups can be calculated using the intensity ratios between corresponding symmetric/asymmetric vibrational modes or the ratios of the same mode in different polarization combinations.  $^{21,47,48}$  Here, the SSP and PPP amplitude ratios ( $A_{\rm SSP}/$  $A_{\rm ppp}$ ) for mode 3 (1378 cm<sup>-1</sup>) were calculated to be  $-0.76 \pm$ 0.02 at the DI-H<sub>2</sub>O surface and  $-0.74 \pm 0.02$  at the WR-H<sub>2</sub>O surface. Similarly, the  $A_{SSP}/A_{PPP}$  ratio for mode 2 (1350 cm<sup>-1</sup>) is also within error for the two surfaces, demonstrating that the similarity is not unique to mode 3. While these ratios indicate the molecular orientation is similar at the two aqueous surfaces, the calculation of specific orientations is not performed in this work because unlike commonly probed vibrational regions (e.g., C-H or carbonyl stretching), analysis of the C-F stretching region is complicated by couplings between C-C and C-F vibrational groups and delocalization of vibrational motion.

The difficulty in properly accounting for these effects is highlighted by previous studies of PFNA at the DI- $H_2O$  surface. In the earliest study, Tyrode et al. modeled the C-F intensity at  $1370~{\rm cm}^{-1}$  in the PFNA spectrum as an asymmetric CF<sub>3</sub> vibration and calculated the terminal CF<sub>3</sub> to be tilted  $60^{\circ}-70^{\circ}$  from the surface normal. <sup>21</sup> In a later study, Okuno and co-workers calculated the hyperpolarizability tensor values for delocalized C-F vibrational modes using the B3LYP functional and reached the conclusion PFNA is only tilted  $\sim \! 10^{\circ}$  off surface normal. <sup>22</sup> Interesting, Tyrode and co-workers attempted to calculate the C-F vibrational

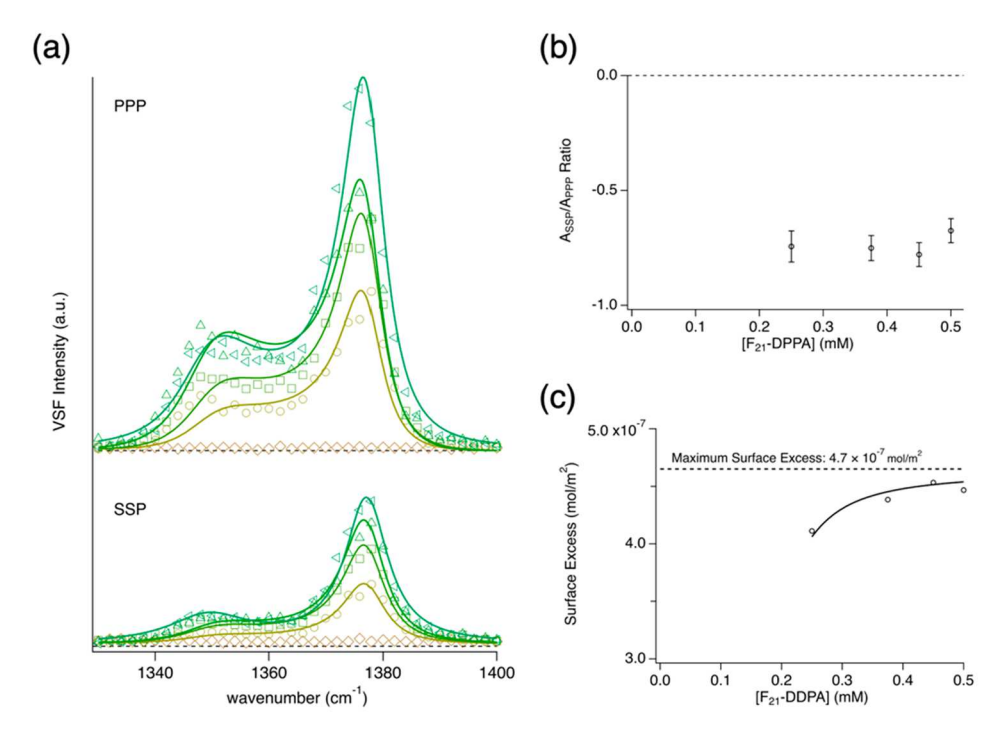


Figure 4. (a) VSF spectra recorded of  $F_{21}$ -DDPA at a basic WR-H<sub>2</sub>O interface recorded in the PPP and SSP polarization combinations at bulk concentrations of 0.15 mM (brown diamonds), 0.25 mM (yellow circles), 0.375 mM (light green squares), 0.45 mM (green upward triangles), and 0.5 mM (dark green right facing triangles). Solid lines are global fits to experimental data. PPP spectra have been vertically shifted for clarity, and the horizontal dashed lines mark zero VSF intensity for each polarization combination. (b)  $A_{SSP}$ :  $A_{PPP}$  ratios for mode 3 calculated from global fits for each concentration. (c)  $F_{21}$ -DDPA surface excess calculated using the  $A_{SSP}$  ratios and the maximum surface excess (horizontal dashed line, 4.7 ×  $10^{-7}$  mol/m<sup>2</sup>) derived from the ML fit.

response using the B3LYP functional but report a lack of accuracy in the calculated frequencies. In this work, we attempted to perform DFT calculations and, similar to Tyrode et al., found the calculated vibrational frequencies were a poor match to experimentally measured frequencies. A calculated infrared spectrum is provided alongside an ATR-FTIR spectrum in the Supporting Information as an example of the frequency mismatch. Given the differing accounts of the accuracy of DFT calculations that have resulted in significantly different physical interpretations of the molecular tilt angle, it remains an open question as to how to best calculate molecular orientations using VSF spectra of the C-F stretching region.

Nonetheless, while procedures for calculating exact orientations from C-F stretching VSF data need development, physical characteristics of F<sub>21</sub>-DDPA that can be drawn out of the data presented in Figure 3 remain promising for the application of VSF to PFAS studies at environmental surfaces. The similarity of the  $A_{\rm SSP}/A_{\rm PPP}$  ratios indicates that the orientation of F21-DDPA is similar at the DI-H2O and WR-H<sub>2</sub>O interfaces. If the molecular orientation were to be insensitive to changes in concentration, then any changes in VSF signal intensity could be directly correlated to the surface concentration of  $F_{21}$ -DDPA. To test the possibility of measuring adsorption isotherms at complex aquatic interfaces, we measured the C-F spectrum for several concentrations of F<sub>21</sub>-DDPA in the SSP and PPP polarization combinations at the basic WR-H<sub>2</sub>O surface (Figure 4a,b). These concentrations (0.15-0.5 mM F<sub>21</sub>-DDPA) and solution conditions were chosen to match the concentration range of the rise and plateau of WR-H<sub>2</sub>O surface pressure isotherm that exhibited the least complicated adsorption behavior.

Resonant C-F vibrational modes were observed for each F<sub>21</sub>-DDPA solution with the exception of the 0.15 mM solution, likely because the surface concentration was below the detection limit at this bulk concentration. Strategies exist that can increase the sensitivity of VSF and are worth further investigation. In the present study, however, we focused on whether the intensity changes originate from either a change in orientational ordering and/or a change in the surface population. Thus, all spectra were globally fit (solid lines in Figure 4) to determine whether the molecular orientation was sensitive to changes in the concentration. The  $A_{CCD}/A_{DDD}$  ratio of mode 3 was calculated for each F21-DDPA concentration and found to be invariant with changes in the bulk concentration (Figure 4c), indicating the orientation of the interfacial PFAS is insensitive to shifts in the concentration. This invariance in molecular orientation is consistent with the invariance in PFNA orientation observed by Tyrode and coworkers.<sup>21</sup> Therefore, the VSF amplitude of mode 3 can be used as a probe of changes in the surface population and provides a measure of changes in F21-DDPA surface density amidst background DOM.

Knowing that the molecular orientation is invariant with changes in the bulk concentration, mode 3 was used to calculate the surface density of  $F_{21}$ -DDPA amidst background DOM. To do this, a modified Langmuir (ML) adsorption model was used to estimate the surface excess from VSF data, which was then used to calculate the surface excess for each bulk concentration. This model (described in the Supporting Information) has been previously used to build adsorption isotherms from second-harmonic and VSF spectroscopic data and is used here to demonstrate the potential of VSF spectroscopy to measure adsorption isotherms of PFAS at

complex aquatic surfaces. 49-51 From the ML, the maximum surface excess was calculated to be 4.7 ( $\pm 2.5$ )  $\times$  10<sup>-7</sup> mol/m<sup>2</sup>, corresponding to a maximum surface density of 357 Å<sup>2</sup>/F<sub>21</sub>-DDPA molecule. While the error in the calculated maximum surface excess is significant, additional fits with similar accuracy generated lower maximum surface excess values. Therefore, 4.7  $\times$  10<sup>-7</sup> mol/m<sup>2</sup> provides an upper bound on the F<sub>21</sub>-DDPA surface concentration. Using this calculated maximum surface excess, the VSF amplitudes of mode 3 were converted to surface concentrations (Figure 4d). The SSP polarization combination was used for this calculation as it only probes the perpendicular component of interfacial dipoles and does not have as many contributions as the PPP polarization combination.<sup>17</sup> For the concentrations that contained measurable C-F resonances, the F<sub>21</sub>-DDPA surface concentration was calculated to increase from  $(4-4.5) \times 10^{-7}$  mol/m<sup>2</sup>.

It is notable that the surface excess values calculated from VSF data are approximately 1 order of magnitude lower than those calculated from surface tension measurements. Despite the error in the VSF derived maximum surface excess that is used to calculate the surface concentrations, the discrepancy in surface concentrations from the two methods can be found in the details of the experimental methods. Surface concentrations calculated from surface tension data will be overestimations as a consequence of DOM adsorbing to the surface alongside F<sub>21</sub>-DDPA. The presence of DOM at the WR-H<sub>2</sub>O surface in our surface tension measurements is supported by the reduced surface tension value of the bare WR-H<sub>2</sub>O surface. Thus, F<sub>21</sub>-DDPA's true surface concentration will be lower than any values derived from the surface tension experiments. For the VSF spectroscopic data, the spectra record only the changing surface population of F<sub>21</sub>-DDPA, despite DOM being present in solution, and the values calculated from the spectroscopic data are specific to F<sub>21</sub>-DDPA. Therefore, these experiments demonstrate that VSF spectroscopy can isolate PFAS vibrational signatures at natural environmental interfaces and suggest that this surface spectroscopic technique is worth further consideration as a potential probe of PFAS adsorption at complex aqueous surfaces.

# CONCLUSION

Understanding PFAS adsorption at naturally occurring aquatic surfaces would be advantageous by an experimental methodology that could isolate a PFAS specific signature amidst a potentially complicated background response. While surface tensiometry can provide important experimental insights into PFAS adsorption behavior in laboratory settings, the experimental results are not guaranteed to neatly map back onto the PFAS adsorption at complex environmental surfaces. Therefore, there is an opportunity to develop experimental techniques and methodologies to probe PFAS at complex aqueous surfaces with molecular specificity.

In this paper, we have demonstrated that VSF spectroscopy has the potential to be one such experimental probe of PFAS adsorption behavior at natural environmental interfaces. Focusing on polyfluorinated dodecylphosphonic acid as a model PFAS, we have illustrated how surface tensiometry is an appropriate experimental technique under well-controlled laboratory conditions. But once the aqueous subphase included unknown background DOM content, the experimental conclusions are frustrated by the coadsorption of DOM. Results from VSF experiments, however, are shown to exclusively report on interfacial F<sub>21</sub>-DDPA species at both

the DI- $H_2O$  and the WR- $H_2O$  surfaces. The unique nature of the C–F stretching vibrational region allows for the isolation of PFAS specific signatures amidst any interfering vibrational response that could have come from the river water DOM. VSF spectra revealed that the complex aquatic matrix of WR- $H_2O$  does not alter the interfacial organization of  $F_{21}$ -DDPA relative to its structure at the simplified DI- $H_2O$  surface. Further experiments found that the orientation of  $F_{21}$ -DDPA at the WR- $H_2O$  surface was invariant to changes in the bulk concentration, indicating VSF signal intensity could be directly correlated to  $F_{21}$ -DDPA surface concentration. As a result, the surface concentration of  $F_{21}$ -DDPA was able to be calculated from VSF data, revealing the true surface coverage of  $F_{21}$ -DDPA was approximately an order of magnitude lower than that calculated from surface tension measurements.

It is important to note that the F<sub>21</sub>-DDPA concentrations studied here are significantly higher than the PFAS concentrations measured in even the most highly contaminated water sources. The lowest concentrations studied, herein, are on the order of 10s of mg/L, larger than the concentrations found in the most highly contaminated water sources by an order of magnitude or more. However, with increased sensitivity, VSF spectroscopy could be applied to the study of PFAS within environmentally relevant concentration ranges. Such sensitivity increases can be achieved with heterodyne VSF experimental setups, 52 through tuning the incident angles of the VIS and IR beams at the air-water interface<sup>53</sup> and leveraging a total internal reflection geometry at other aqueous environmental interfaces (e.g., oil-water).54 These sensitivity increases would also aid in measuring a more complete adsorption isotherm, reducing the error in the calculated maximum surface excess. Nonetheless, this work has demonstrated that VSF is an experimental methodology capable of probing the interfacial behavior of PFAS pollutants at natural environmental interfaces. Such future studies could provide invaluable insight into how complex aquatic matrices alter the adsorption behavior of PFAS relative to controlled laboratory systems.

#### ASSOCIATED CONTENT

#### Supporting Information

The Supporting Information is available free of charge at https://pubs.acs.org/doi/10.1021/acs.jpca.3c01487.

Historic Willamette River water quality report, CMC calculations, VSF fit parameters, comparison of calculated and experimental IR spectra, application of modified Langmuir adsorption model to VSF data (PDF)

## AUTHOR INFORMATION

#### **Corresponding Author**

Andrew P. Carpenter — School of Chemical, Biological, and Environmental Engineering, Oregon State University, Corvallis, Oregon 97331, United States; orcid.org/0000-0003-1020-1706; Email: carpeand@oregonstate.edu

#### Authors

Jade N. White — School of Chemical, Biological, and Environmental Engineering, Oregon State University, Corvallis, Oregon 97331, United States; ⊚ orcid.org/0009-0005-7408-9938

- Annemarie Hasbrook School of Chemical, Biological, and Environmental Engineering, Oregon State University, Corvallis, Oregon 97331, United States; Orcid.org/0009-0007-1554-8115
- Makenna Reierson School of Chemical, Biological, and Environmental Engineering, Oregon State University, Corvallis, Oregon 97331, United States; ◎ orcid.org/0009-0007-8989-9700
- Joe E. Baio School of Chemical, Biological, and Environmental Engineering, Oregon State University, Corvallis, Oregon 97331, United States

Complete contact information is available at: https://pubs.acs.org/10.1021/acs.jpca.3c01487

#### **Notes**

The authors declare no competing financial interest.

## ACKNOWLEDGMENTS

This work was supported by the National Science Foundation Ascend Postdoctoral Research Fellowship under Grant 2137997.

## REFERENCES

- (1) Duchesne, A. L.; Brown, J. K.; Patch, D. J.; Major, D.; Weber, K. P.; Gerhard, J. I. Remediation of PFAS-Contaminated Soil and Granular Activated Carbon by Smoldering Combustion. *Environ. Sci. Technol.* **2020**, *54* (19), 12631–12640.
- (2) Li, F.; Duan, J.; Tian, S.; Ji, H.; Zhu, Y.; Wei, Z.; Zhao, D. Shortchain per- and polyfluoroalkyl substances in aquatic systems: Occurrence, impacts and treatment. *Chem. Eng. J.* **2020**, 380, 122506.
- (3) Lyu, X.; Xiao, F.; Shen, C.; Chen, J.; Park, C. M.; Sun, Y.; Flury, M.; Wang, D. Per- and Polyfluoroalkyl Substances (PFAS) in Subsurface Environments: Occurrence, Fate, Transport, and Research Prospect. *Reviews of Geophysics* **2022**, *60* (3), No. e2021RG000765.
- (4) Trang, B.; Li, Y.; Xue, X.-S.; Ateia, M.; Houk, K. N.; Dichtel, W. R. Low-temperature mineralization of perfluorocarboxylic acids. *Science* **2022**, *377* (6608), 839–845.
- (5) Bangma, J.; Eaves, L. A.; Oldenburg, K.; Reiner, J. L.; Manuck, T.; Fry, R. C. Identifying Risk Factors for Levels of Per- and Polyfluoroalkyl Substances (PFAS) in the Placenta in a High-Risk Pregnancy Cohort in North Carolina. *Environ. Sci. Technol.* **2020**, *54* (13), 8158–8166.
- (6) Pétré, M.-A.; Genereux, D. P.; Koropeckyj-Cox, L.; Knappe, D. R. U.; Duboscq, S.; Gilmore, T. E.; Hopkins, Z. R. Per- and Polyfluoroalkyl Substance (PFAS) Transport from Groundwater to Streams near a PFAS Manufacturing Facility in North Carolina, USA. *Environ. Sci. Technol.* **2021**, 55 (9), 5848–5856.
- (7) Drinking Water Health Advisories for PFOA and PFOS, EPA, 2022. https://www.epa.gov/sdwa/drinking-water-health-advisories-pfoa-and-pfos (accessed 2023-3-10).
- (8) Hale, S. E.; Arp, H. P. H.; Slinde, Gør. A.; Wade, E. J.; Bjørseth, K.; Breedveld, G. D.; Straith, B. F.; Moe, K. G.; Jartun, M.; Høisæter, Å. Sorbent amendment as a remediation strategy to reduce PFAS mobility and leaching in a contaminated sandy soil from a Norwegian firefighting training facility. *Chemosphere* **2017**, *171*, 9–18.
- (9) Høisæter, Å.; Pfaff, Å.; Breedveld, G. D. Leaching and transport of PFAS from aqueous film-forming foam (AFFF) in the unsaturated soil at a firefighting training facility under cold climatic conditions. *Journal of Contaminant Hydrology* **2019**, 222, 112–122.
- (10) Lyu, Y.; Brusseau, M. L.; Chen, W.; Yan, N.; Fu, X.; Lin, X. Adsorption of PFOA at the Air-Water Interface during Transport in Unsaturated Porous Media. *Environ. Sci. Technol.* **2018**, *52* (14), 7745–7753.
- (11) Schaefer, C. E.; Lemes, M. C. S.; Schwichtenberg, T.; Field, J. A. Enrichment of poly- and perfluoroalkyl substances (PFAS) in the

- surface microlayer and foam in synthetic and natural waters. *J. Hazard. Mater.* **2022**, 440, 129782.
- (12) Schwichtenberg, T.; Bogdan, D.; Carignan, C. C.; Reardon, P.; Rewerts, J.; Wanzek, T.; Field, J. A. PFAS and Dissolved Organic Carbon Enrichment in Surface Water Foams on a Northern U.S. Freshwater Lake. *Environ. Sci. Technol.* **2020**, *54* (22), 14455–14464.
- (13) Surette, M. C.; Nason, J. A.; Harper, S. L.; Mitrano, D. M. What is "Environmentally Relevant"? A framework to advance research on the environmental fate and effects of engineered nanomaterials. *Environmental Science: Nano* **2021**, 8 (9), 2414–2429.
- (14) Schaefer, C. E.; Culina, V.; Nguyen, D.; Field, J. Uptake of Poly- and Perfluoroalkyl Substances at the Air-Water Interface. *Environ. Sci. Technol.* **2019**, *53* (21), 12442–12448.
- (15) Wegner, C.; Hamburger, M. Occurrence of Stable Foam in the Upper Rhine River Caused by Plant-Derived Surfactants. *Environ. Sci. Technol.* **2002**, *36* (15), 3250–3256.
- (16) Brusseau, M. L.; Van Glubt, S. The influence of molecular structure on PFAS adsorption at air-water interfaces in electrolyte solutions. *Chemosphere* **2021**, *281*, 130829.
- (17) Lambert, A. G.; Davies, P. B.; Neivandt, D. J. Implementing the Theory of Sum Frequency Generation Vibrational Spectroscopy: A Tutorial Review. *Appl. Spectrosc. Rev.* **2005**, *40* (2), 103–145.
- (18) Geiger, F. M. Second Harmonic Generation, Sum Frequency Generation, and  $\chi(3)$ : Dissecting Environmental Interfaces with a Nonlinear Optical Swiss Army Knife. *Annu. Rev. Phys. Chem.* **2009**, *60* (1), 61–83.
- (19) Beaman, D. K.; Robertson, E. J.; Richmond, G. L. Ordered Polyelectrolyte Assembly at the Oil-Water Interface. *Proc. Natl. Acad. Sci. U. S. A.* **2012**, *109*, 3226–3231.
- (20) Ohno, P. E.; Wang, H.-f.; Geiger, F. M. Second-order spectral lineshapes from charged interfaces. *Nat. Commun.* **2017**, *8* (1), 1032.
- (21) Tyrode, E.; Johnson, C. M.; Rutland, M. W.; Day, J. P. R.; Bain, C. D. A Study of the Adsorption of Ammonium Perfluorononanoate at the Air-Liquid Interface by Vibrational Sum-Frequency Spectroscopy. *J. Phys. Chem. C* **2007**, *111* (1), 316–329.
- (22) Okuno, M.; Homma, O.; Kuo, A.-T.; Urata, S.; Koguchi, R.; Miyajima, T.; Ishibashi, T.-A. Molecular Orientations and Conformations of Air/Fluoroalkyl Acrylate Polymer Interfaces Studied by Heterodyne-Detected Vibrational Sum Frequency Generation. *Macromolecules* **2019**, 52 (22), 8705–8712.
- (23) Neese, F. The ORCA program system. WIREs Computational Molecular Science 2012, 2 (1), 73–78.
- (24) Neese, F. Software update: The ORCA program system—Version 5.0. WIREs Computational Molecular Science 2022, 12 (5), No. e1606.
- (25) Lee, C.; Yang, W.; Parr, R. G. Development of the Colle-Salvetti correlation-energy formula into a functional of the electron density. *Phys. Rev. B* **1988**, 37 (2), 785–789.
- (26) Becke, A. D. Density-functional thermochemistry. III. The role of exact exchange. *J. Chem. Phys.* **1993**, *98*, 5648–5652.
- (27) Monde, K.; Miura, N.; Hashimoto, M.; Taniguchi, T.; Inabe, T. Conformational Analysis of Chiral Helical Perfluoroalkyl Chains by VCD. *J. Am. Chem. Soc.* **2006**, *128* (18), 6000–6001.
- (28) Freedman, L. D.; Doak, G. O. The Preparation And Properties Of Phosphonic Acids. *Chem. Rev.* **1957**, *57* (3), 479–523.
- (29) Rosen, M. J. Surfactants and Interfacial Phenomena; Wiley-Interscience: 2004.
- (30) Silva, J. A. K.; Martin, W. A.; McCray, J. E. Air-water interfacial adsorption coefficients for PFAS when present as a multi-component mixture. *Journal of Contaminant Hydrology* **2021**, 236, 103731.
- (31) Di Anibal, C. V.; Moroni, M. A.; Verdinelli, V.; Rodríguez, J. L.; Minardi, R.; Schulz, P. C.; Vuano, B. Critical micelle concentration of tridecane, tetradecane and hexadecane phosphonic acids and their mono- and disodium salts. *Colloids Surf., A* **2009**, 348 (1), 276–281.
- (32) Rehfeld, S. J. Adsorption of sodium dodecyl sulfate at various hydrocarbon-water interfaces. *J. Phys. Chem.* **1967**, 71 (3), 738–745. (33) Gillap, W. R.; Weiner, N. D.; Gibaldi, M. Ideal behavior of sodium alkyl sulfates at various interfaces. Thermodynamics of

adsorption at the oil-water interface. J. Phys. Chem. 1968, 72, 2222.

- (34) Lu, J. R.; Thomas, R. K.; Penfold, J. Surfactant layers at the air/water interface: structure and composition. *Adv. Colloid Interface Sci.* **2000**, *84* (1), 143–304.
- (35) Shinoda, K.; Hato, M.; Hayashi, T. Physicochemical properties of aqueous solutions of fluorinated surfactants. *J. Phys. Chem.* **1972**, *76* (6), 909–914.
- (36) Mukerjee, P.; Handa, T. Adsorption of fluorocarbon and hydrocarbon surfactants to air-water, hexane-water and perfluorohexane-water interfaces. Relative affinities and fluorocarbon-hydrocarbon nonideality effects. *J. Phys. Chem.* **1981**, *85* (15), 2298–2303.
- (37) Nakayama, H.; Shinoda, K. z. The Effect of Added Salts on the Solubilities and Krafft Points of Sodium Dodecyl Sulfate and Potassium Perfluoro-octanoate. *Bull. Chem. Soc. Jpn.* **1967**, 40 (8), 1797–1799.
- (38) Taylor, D. J. F.; Thomas, R. K.; Li, P. X.; Penfold, J. Adsorption of Oppositely Charged Polyelectrolyte/Surfactant Mixtures. Neutron Reflection from Alkyl Trimethylammonium Bromides and Sodiume Poly(styrenesulfonate) at the Air/Water Interface: The Effect of Surfactant Chain Length. *Langmuir* 2003, 19, 3712–3719.
- (39) Schabes, B. K.; Altman, R. M.; Richmond, G. L. Come Together: Molecular Details into the Synergistic Effects of Polymer-Surfactant Adsorption at the Oil/Water Interface. *J. Phys. Chem. B* **2018**, *122* (36), 8582–8590.
- (40) Penfold, J.; Staples, E.; Thompson, L.; Tucker, I.; Hines, J.; Thomas, R. K.; Lu, J. R.; Warren, N. Structure and Composition of Mixed Surfactant Micelles of Sodium Dodecyl Sulfate and Hexaethylene Glycol Monododecyl Ether and of Hexadecyltrimethylammonium Bromide and Hexaethylene Glycol Monododecyl Ether. *J. Phys. Chem. B* 1999, 103 (25), 5204–5211.
- (41) Golbek, T. W.; Franz, J.; Elliott Fowler, J.; Schilke, K. F.; Weidner, T.; Baio, J. E. Identifying the selectivity of antimicrobial peptides to cell membranes by sum frequency generation spectroscopy. *Biointerphases* **2017**, *12* (2), 02D406.
- (42) Ghosh, N.; Roy, S.; Mondal, J. A. Headgroup-Specific Interaction of Biological Lipid Monolayer/Water Interface with Perfluorinated Persistent Organic Pollutant (f-POP): As Observed with Interface-Selective Vibrational Spectroscopy. *J. Phys. Chem. B* **2022**, *126* (2), 563–571.
- (43) Socrates, G. Infrared and Raman Characteristic Group Frequencies: Tables and Charts; John Wiley & Sons Ltd.: 2001.
- (44) Even, M. A.; Lee, S.-H.; Wang, J.; Chen, Z. Detection and Spectral Analysis of Trifluoromethyl Groups at a Surface by Sum Frequency Generation Vibrational Spectroscopy. *J. Phys. Chem. B* **2006**, *110* (51), 26089–26097.
- (45) Kristalyn, C. B.; Lu, X.; Weinman, C. J.; Ober, C. K.; Kramer, E. J.; Chen, Z. Surface Structures of an Amphiphilic Tri-Block Copolymer in Air and in Water Probed Using Sum Frequency Generation Vibrational Spectroscopy. *Langmuir* **2010**, 26 (13), 11337–11343.
- (46) Volpati, D.; Chachaj-Brekiesz, A.; Souza, A. L.; Rimoli, C. V.; Miranda, P. B.; Oliveira, O. N.; Dynarowicz-Łątka, P. Semifluorinated thiols in Langmuir monolayers A study by nonlinear and linear vibrational spectroscopies. *J. Colloid Interface Sci.* **2015**, 460, 290–302.
- (47) Hirose, C.; Akamatsu, N.; Domen, K. Formulas for the Analysis of the Surface SFG Spectrum and Transformation Coefficients of Cartesian SFG Tensor Components. *Appl. Spectrosc.* **1992**, *46* (6), 1051–1072.
- (48) Zhuang, X.; Miranda, P. B.; Kim, D.; Shen, Y. R. Mapping molecular orientation and conformation at interfaces by surface nonlinear optics. *Phys. Rev. B* **1999**, *59* (19), 12632–12640.
- (49) Wang, H.; Yan, E. C. Y.; Liu, Y.; Eisenthal, K. B. Energetics and Population of Molecules at Microscopic Liquid and Solid Surfaces. *J. Phys. Chem. B* **1998**, *102* (23), 4446–4450.
- (50) de Aguiar, H. B.; de Beer, A. G. F.; Strader, M. L.; Roke, S. The Interfacial Tension of Nanoscopic Oil Droplets in Water Is Hardly Affected by SDS Surfactant. *J. Am. Chem. Soc.* **2010**, *132* (7), 2122–2123.
- (51) Carpenter, A. P.; Foster, M. J.; Jones, K. K.; Richmond, G. L. Effects of Salt-Induced Charge Screening on AOT Adsorption to the

ī

- Planar and Nanoemulsion Oil-Water Interfaces. Langmuir 2021, 37 (29), 8658-8666.
- (52) Stiopkin, I. V.; Jayathilake, H. D.; Bordenyuk, A. N.; Benderskii, A. V. Heterodyne-Detected Vibrational Sum Frequency Generation Spectroscopy. *J. Am. Chem. Soc.* **2008**, *130* (7), 2271–2275.
- (53) Hore, D. K.; Tyrode, E. Probing Charged Aqueous Interfaces Near Critical Angles: Effect of Varying Coherence Length. *J. Phys. Chem. C* 2019, 123 (27), 16911–16920.
- (54) Löbau, J.; Wolfrum, K. Sum-frequency spectroscopy in total internal reflection geometry: signal enhancement and access to molecular properties. *J. Opt. Soc. Am. B* **1997**, *14* (10), 2505–2512.